The Gamma Intensity Monitor at the Crystal-Barrel-Experiment

by

William R. McGehee

Submitted to the Department of Physics
in partial fulfillment of the requirements for the degree of

Bachelor of Science in Physics

at the

MASSACHUSETTS INSTITUTE OF TECHNOLOGY

June 2008

Author .....
Department of Physics
May 9, 2008

Certified by .....
Bernd Surrow
Associate Professor of Physics
Thesis Supervisor

Accepted by .....
David E. Pritchard
Thesis Coordinator

The Gamma Intensity Monitor at the Crystal-Barrel-Experiment

by

William R. McGehee

Submitted to the Department of Physics
on May 9, 2008, in partial fulfillment of the
requirements for the degree of
Bachelor of Science in Physics

Abstract

This thesis details the motivation, design, construction, and testing of the Gamma Intensity Monitor (GIM) for the Crystal-Barrel-Experiment at the Universität Bonn. The CB-ELSA collaboration studies the baryon excitation spectrum; resonances are produced by exciting nucleons in a polarized target with a linearly or circularly polarized, GeV-order photon beam. The photoproduced decay states are measured by a variety of detectors covering almost 4π of the solid angle about the target.

To measure the total cross section of these reactions, the total flux of photons through the target must be known to high accuracy. As the total cross section for nuclear photoproduction is low, counting the photons unscattered in the target is sufficiently accurate measurement of this quantity–this is the purpose of the Gamma Intensity Monitor. It is the final detector along the beam path and counts all photons that do not react with the target.

The major design parameter is that the detector must consistently count GeV order photons at 10 MHz. This is accomplished by allowing the gammas to electron-positron pair produce within Ĉerenkov radiating PbF_2 crystals. The Ĉerenkov light from these highly relativistic lepton pairs is measured with industrial photomultiplier tubes to provide an effective efficiency close to unity. Special bases were built for photomultiplier to ensure stable signal amplification even high count rates.

Detailed descriptions of the GIM are provided to ensure that its inner working are completely transparent and to enable efficient operation and maintenance of the detector.

Thesis Supervisor: Bernd Surrow
Title: Associate Professor of Physics

Acknowledgments

The story behind this thesis involves a large number of people. First and foremost, I would like to thank Christoph Wendel and Ulrike Thoma for their unending patience, encouragement, and advice throughout my time in Bonn; without them none of this would have been possible. To Aaron McVeigh and Jessica Dielmann with whom I worked on designing and rebuilding the GIM, I thank you for the great times we had together. To the rest of the Helmoltz Institut für Strahlung und Kernphysik, I want you to know that your community is the warmest and most welcoming I have ever encountered and it was you who truly made my summer.

Contents

List of Figures

List of Tables

Chapter 1

Introduction

1.1 Motivation

This thesis explains in detail the motivation, design, construction, and testing of the Gamma Intensity Monitor (GIM) built for the Crystal-Barrel-Collaboration during the summer of 2007. The detector's main task is to robustly count γ's at 10MHz. This thesis provides the the information relevant to understanding the inner workings of the detector so that it may easily be used, fixed, and adapted with minimal surprises.

For those who are new to the experiment or those looking at the experiment from a historical perspective, the experiment setup is described as it stood during mid-2007. It is hoped that this document may be of some use to future summer researchers in the Crystal-Barrel-Collaboration.

1.2 The Crystal-Barrel-Experiment at a Glance

The Crystal-Barrel-Collaboration explores nucleon resonances by bombarding low mass nuclei with GeV-order photons. The experimental setup is well suited to find resonances over a wide range of photon energies and can measure both differential and total cross sections of these resonances. The γ's used to excite these baryon resonances are Bremsstrahlung produced from a high energy electron beam incident on a radiator target. The γ's produced in this manner are tagged in energy by

measuring the momentum loss of their associated electrons. The tagged beam of γ's is then collimated and incident upon the cryogenically cooled target of liquid hydrogen or butanol. The target is surrounded by a variety of detectors that measure the angular distribution and energy of the decay states of the photoproduced events in the target. This allows for the event to be reconstructed and for differential cross sections to be determined.

To determine the total cross section of these resonances, the total flux of γ's through the target must be known. Information from the photon tagging system is not enough to do this as the beam is collimated before it strikes the target. Only a small fraction of the γ's scatter in the target, so a very accurate count of the flux of photons at the target can be determined by counting the unscattered γ's.

1.3 Physical Background

The baryon resonance found by examining the decay products of these collisions are interesting for several reasons. First, the spectrum of baryon resonances (a part of which is show in Figure 1-1) is not completely understood. Many models exist, but they often predict many more states than have been observed and do not accurately describe the ones that have been found. The energy range probed by the Crystal-Barrel-Experiment is too high for simple perturbations of QCD to remain valid. Other models involve instanton-induced quark forces or ideas of chiral symmetry breaking which are active areas of interest. There is also work being done on in-medium modification of meson masses[11].

Previous studies of baryon resonances have used π's as the exciting particles, but the cross sections for Nπ scattering are very low and it is experimentally unfeasible to continue exploring the baryon spectrum in this fashion[13]. Luckily γ's have much higher total cross sections and provide a reasonable means for accessing these states.

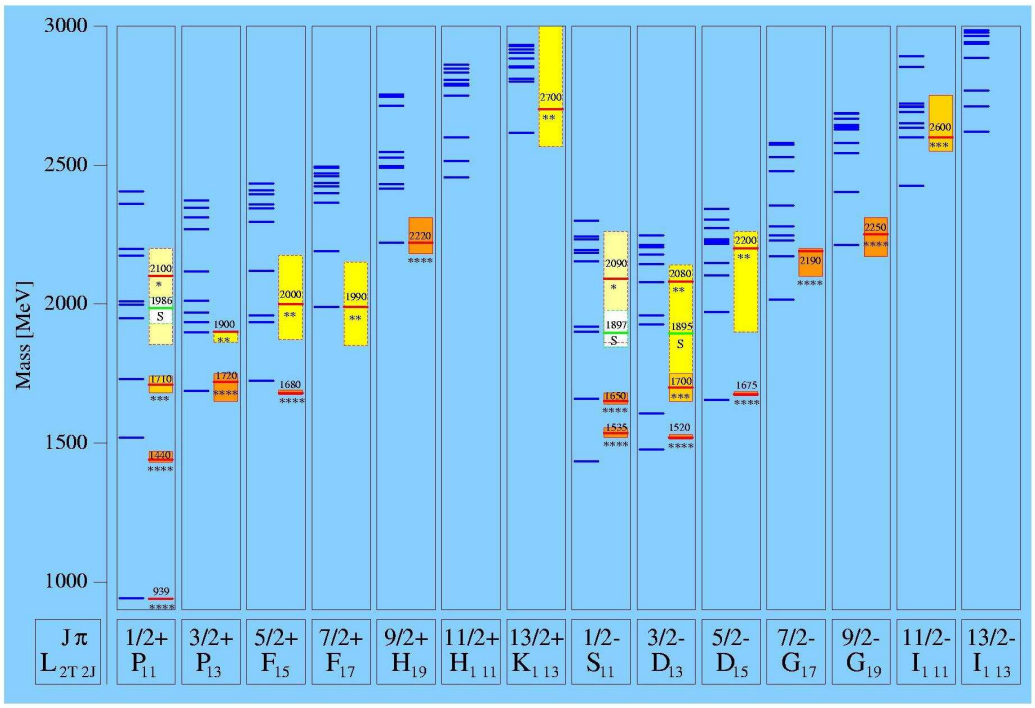

Figure 1-1: Spectra of observed(left) and predicted(right) N* resonances (S = $\frac{1}{2}$)[12]

Chapter 2

Overview of the Crystal-Barrel-Experiment

The Crystal-Barrel-Experiment is a medium energy, nuclear physics collaboration located at the Universität Bonn. The groups consists of members from the Universität Bonn, Ruhr-Universität Bochum, Universität Giessen, Universität Basel, Florida State University, and the PNPI at Gatchina. The main research interest is the study of γ-induced nucleon resonances that probe the baryon spectrum in a useful and novel fashion. High energy γ's are produced by bremsstrahlung of electrons accelerated in the ELSA accelerator. An array of detectors is used to characterize the incident γ's and provide detailed spatial, charge, and energy information to describe the decay states they produce.

The basic layout of the experiment is show in Figure 2-1. The electron beam from ELSA enters from the right and collides with a foil producing bremsstrahlung photons. The energies of these photons is measured by a magnetic spectrometer that bends the scattered electrons toward an array of scintillator detectors, separating them based on their momenta. The photon beam travels through a collimator towards the target; a Møller polarimeter at this stage can also be used to measure the degree of electron beam polarization. If the γ photoproduces off the target nuclei, the final state of this nucleon resonance is measured by an array of detectors covering 97.8% of the 4π solid angle that surround the target and determine the charges and trajectories

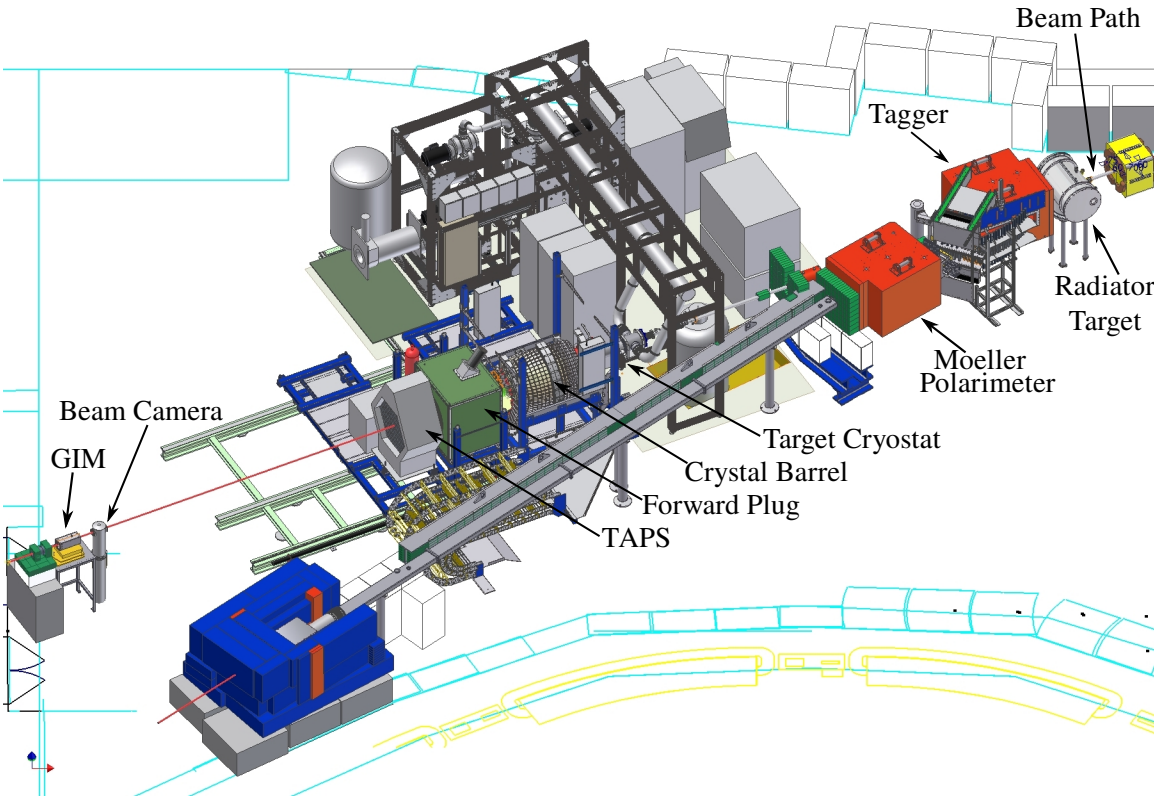

Figure 2-1: Schematic of the Crystal-Barrel-Experiment [1]

of the decay state products. More detectors are placed in the forward direction with higher angular resolution and higher count rate capability since scattering through low angles is more probable due to the high momentum of the center of mass frame. The majority of photons are not scattered in the target and travel toward the photon beam dump where they are counted by the Gamma Intensity Monitor.

What follows is a brief description of the elements of the Crystal-Barrel-Experiment works starting with beam production and progressing linearly through the stages of the experiment.

2.1 ELSA

The ELektronen-Stretcher-Anlage (Electron Stretcher Accelerator) provides beams of electrons at energies from 0.5 to 3.2 GeV for hadron physics and synchrotron

radiation experiments. Based on the requirements of a given run, the beam can be linearly polarized or randomly oriented. The beam starts at a polarized electron gun made from a strained GaAs-like supperlattice irradiated by a circularly polarized laser[6]. The beam is pulsed at 50 Hz based with pulse lengths of 1 microsecond and attains polarizations up to 80% at the source. These electrons are then accelerated down a gun chamber to 120keV. From the gun chamber they are sent into a LINAC and accelerated to 30 MeV at which point they are dumped into a booster synchrotron and accelerated to 1.6 GeV with maximal polarization near 75%. From there they travel in to stretcher ring where they are stored and accelerated up to 3.2 GeV as shown in Figure 2-2. The acceleration frequency in the synchrotron and stretcher ring are 500MHz with bunches 2ns long. Electrons are extracted from the stretcher ring in 6 second long spills with maximal currents up to 100 nA; only 1nA is used for the CB experiment.

To maintain polarization while traveling in the main ring, the electron spins are aligned vertically such that they parallel the field of the turning magnets. Resonances in the stretcher ring are the primary source of loss of polarization with the maximal polarization in the stretcher ring dropping to 65% at 2.5 GeV and 30% at 3.2 GeV. The experiment requires longitudinally polarized spin, so a superconducting solenoid is used to rotate the spins using Larmor precession directly before they strike the radiator target.

2.2 Radiator Target

The GeV-level electrons that leave ELSA are directed toward a target where coherent bremsstrahlung is produced; electrons in the range of 14-96% of the incident beam energy can be tagged in the photon energy tagger. In the case of polarized electrons incident on a polarized radiator target, an asymmetry can be observed in the count rates for scattering into different angles allowing the degree of polarization to be determined.

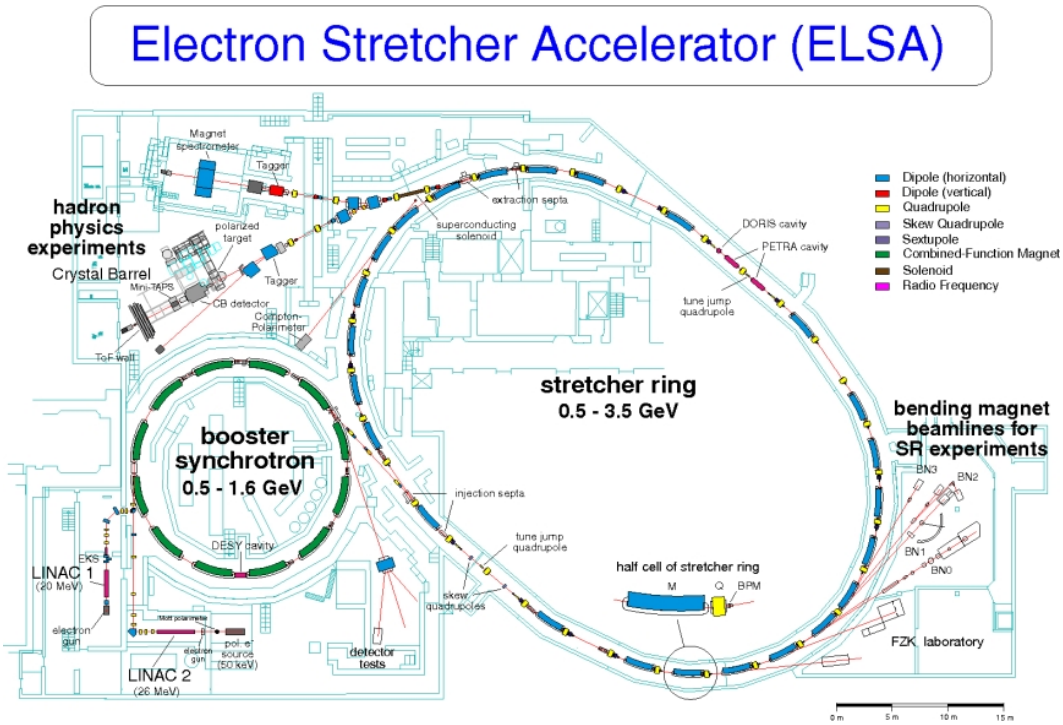

Figure 2-2: Plan of the experimental hall showing components of ELSA and the CB experiment.[1]

2.3 Photon Energy Tagger

To measure the energy of the bremsstrahlung photons produced in the radiator target, a magnetic spectrometer measures the momentum of their associated scattered electrons. As the energy of the beam is well defined, the energy of the photon is found through energy conservation. The tagger is designed to serve as part of the primary trigger for the data collection apparatus as it is imperative to know the energy of the photoproducing γ and to provide a consistent method for timing the event.

The spectrometer consists of a large dipole magnet encapsulating a vacuum chamber described in detail in [3]. The electrons not scattered in the radiator target are deflected by 9° and sent to electron beam dump. Electrons that are scattered in the radiator target are bent toward a series of 96 plastic scintillator bars read out by photomultiplier tubes as shown in Figure 2-3(a). The bars are arranged such that each bar overlaps its neighbors as shown in Figure 2-3(b) to ensure that the energy

range measured is continuous and for each electron to strike two channels for error reduction. This allows a coincidence between adjacent bars to be taken to reduce the rate of false counts from dark current, cosmic rays, or any other source of uncorrelated noise. Due to the physical size of the PMT's compared to the scintillators, adjacent bars are aligned in opposite direction. Further noise reduction is attained from this configuration as the beam is incident upon only a small sliver of the bars chosen equidistant from the photomultipliers in both directions; this keeps adjacent signals very close in the time domain and allows for signals generated in other parts of the scintillators to be discarded from the data set.

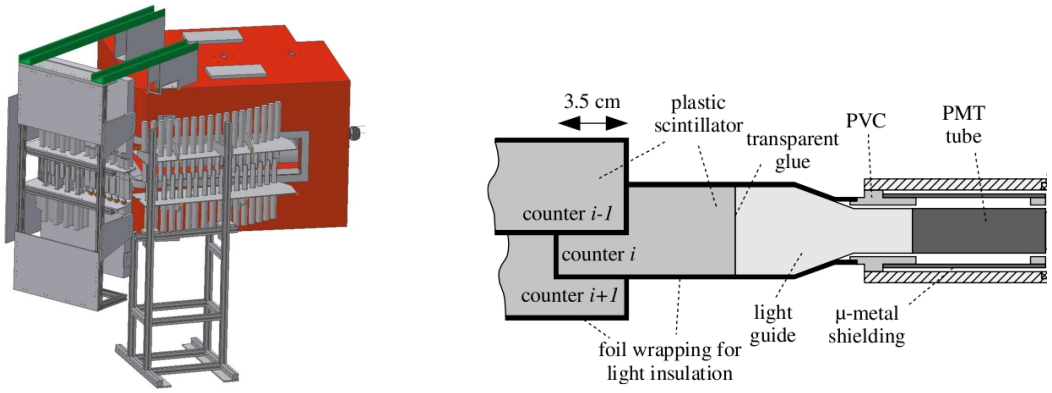

(a) Tagger Schematic[1]

(b) Scintillator Arrangement[3]

Figure 2-3: Diagram of the Tagger

The tagger is very important for determining the proper calibration of the GIM. A photon definition probability for each channel in the tagger can be made that shows the correlation between detecting an electron at the tagger and observing a corresponding signal in the GIM. These correlation probabilities are useful in calibrating thresholds in the GIM electronics and in verifying that the detector is performing as expected. The probabilities measured will have values close to .5; values very close to unity should not be expected as the γ beam is collimated after it leaves the tagger. Knowledge of this tagging efficiency is necessary to determining the total photon flux at the target[3].

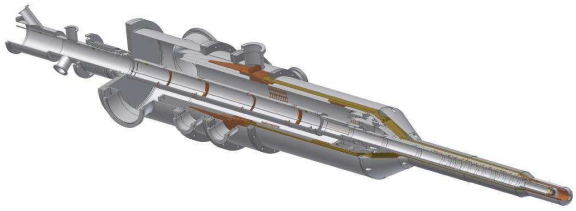

Figure 2-4: Target cryostat[1]

2.4 Møller Detector

The polarization of the electron beam is measured by the Møller detector by utilizing the fact that the differential cross section for elastic electron-electron scattering is helicity dependant. The relative orientation of the target and beam polarizations can be adjusted to further explore the polarization of the beam[7].

2.5 Target

As the purpose of this experiment is to study baryon resonances, the optimal target material would be polarized protons or neutrons. Storing an ensemble of nucleons is not easy, so liquid H_2 and tiny, ultra-cold balls of Butanol are used instead. The target is held within a large stationary cryostat that the crystal barrel slides over with a central cavity left open for the beam path as shown in Figure 2-4. The actual target is 52.84 mm long and 30 mm in diameter with windows made of kapton for high radiation resistance, high strength, and low outgassing rates[13].

To polarize the target, a 5T external magnet can be temporarily placed over the target cryostat when the barrel has been retracted from its measurement position. A 0.64 T field is supplied inside the cryostat for maintaining polarization during data collection and can maintain 70% polarization for 2 days.

2.6 Scintillating Fiber Detector

The scintillating fiber detector, also known as the inner detector, resides just outside the target cryostat and inside of the barrel's scintillating crystals. It is used for

charged particle identification and spatial location of their trajectories. The detector is composed of three layers of organic scintillating fibers wrapped around a 40 cm long, cylindrical holding structure; the fibers are epoxied to carbon fiber tubes to ensure that they remain in their exact wrapped orientations. Each layer has a different fiber orientation, so the particle trajectory can be determined by taking the spatial intersection of the different layers. The inner layer is wrapped in the left-handed direction 24.5° from straight with 157 fibers, the middle layer is wrapped in the opposite direction with 165 fibers, and the outer layer is wrapped with 191 fibers parallel to the beam direction[2]. Each fiber in the first and second layer is wound halfway around the holding structure. The exact location of the event can be determined even if only two of the layers are hit but three is preferred for noise reduction.

Fibers are made from organic scintillators as they have short decay times that allow them to be incorporated into the fast trigger for event reconstruction. The have peak emission at $\lambda = 435nm$ and are optically contacted to photomultipliers outside of the crystal barrel through optical fibers with 70% efficiency. Hamamatsu H6568 PMT's were chosen for their sensitivity over the spectral range of the scintillators and their ability to read out multiple channels in the same PMT. The photocathode of these detectors is divided into a square array of 16, 4mm square pads that can handle count rates of up to 100kHz.

2.7 Crystal-Barrel-Detector

The namesake detector of the experiment is composed of 1230 CsI scintillating crystals arranged around a barrel-shaped cavity in which the target and scintillating fiber detector reside[13]. The purpose of this detector is to provide spatial and energy information for the nucleon resonance decay states to enable construction of differential scattering cross sections for events scattering into the polar angles from 30° to 168°. The crystals cover 6° of polar angle and 6° of azimuthal angle each, and are arranged in a radial orientations as shown in Figure 2-5.

The scintillation light from the crystals (produced in the range of 450-610 nm)

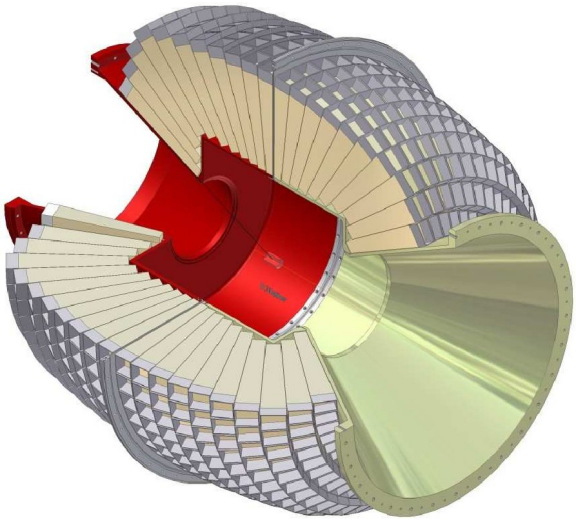

Figure 2-5: Crystal layout in barrel[1]

is read out by photodiodes, but as these diode's optimal efficiency lies around 650 nm, wavelength shifting plates are used to connect the two regions and shift the scintillation light into the appropriate frequency range.

2.8 Crystal-Barrel-Forward-Plug and miniTAPS

To give better spatial and timing resolution for low scattering angles, the Crystal-Barrel-Forward-Plug (CBFP) and the miniTAPS are used. They both consist of crystals read out by high rate PMT's, but miniTAPS has higher angular resolution. The CBFP covers polar angles from 11.5° to 27.5° as shown in Figure 2-6 while the miniTAPS detector covers the rest of the space down to 1.5° from the beam line. The channels in the CBFP and miniTAPS have plastic scintillators in front of their crystals which are read out by wavelength-shifting fibers; these are used for charged particle identification and as a veto mechanism for each channel.

2.9 Beam Camera

Directly before the GIM, a camera is mounted to measure the geometric profile and location of the beam. It is located as far away from the beam collimator as possible to

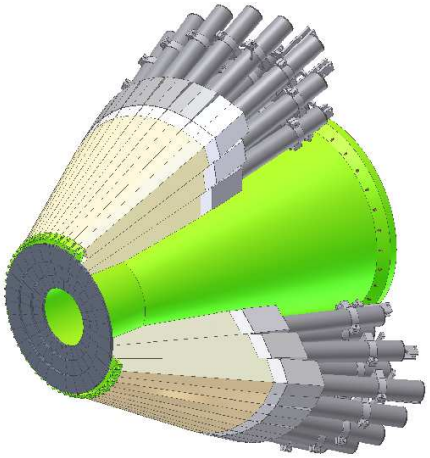

Figure 2-6: Forward Plug[1]

improve its spatial resolution; maximal precision of beam center can be determined to 0.1 mm. The efficiency of the detector is very low, so it is only useful in determining the shape and position of the beam profile and for feedback when controlling beam position.

2.10 The Original Gamma Intensity Monitor

The Gamma Intensity Monitor was designed to efficiently count the γ's not scattered in the target; as the scattering probability is low, this gives a accurate measure of the total flux of γ's and enables total cross section measurements to be made. Its first and second incarnations were build by Michael Konrad during his Diplom and graduate studies at Bonn. His Diplom thesis details the first version[9], but the second detector was and remains undocumented. The detector sat directly downstream of the beam camera and worked by measuring the Ĉerenkov light from electron-positron pairs produced from γ decay in lead glass crystals. Standard photomultiplier tubes were used to measure this Ĉerenkov light, and special high rate bases were designed to handle the expected rates at the detector. All of these pieces were enclosed in a box 145 mm square and roughly 420 mm long made of 10 mm thick aluminum plates. The front cover of the detector through which the photon beam entered was covered

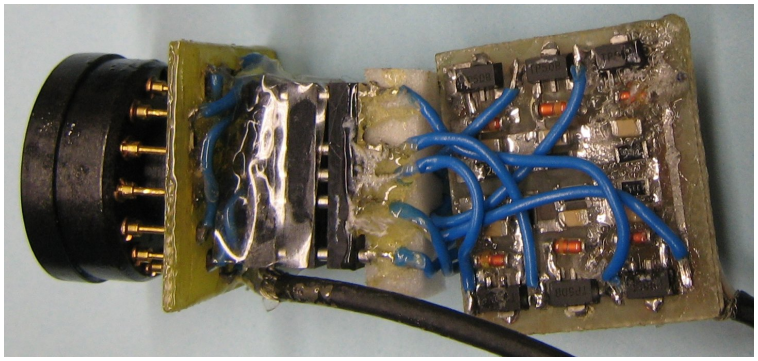

Figure 2-7: Image of old PMT base design

by a rigid, opaque plastic plate to reduce scattering at this surface; the rear (facing the beam dump) was left open.

Specifically, the box contained a square, 4×4 array of lead fluoride crystals optically contacted to Photonis XP2900 PMT's. The bases for the PMT's were built in-house on two boards connected by standard pin header and wires with loose components epoxied in place as shown in Figure 2-7. The exposed components such as the pin header and some of the wires in this design were overly delicate, and many of these had failed by mid-2007. Each of the bases was different in construction and exhibited a unique failure mode. They were often impossible to repair as they had been covered in epoxy.

For a period of time the GIM was operated in a limited state using only the central four channels (positions 6, 7, 10, and 11 as shown in Figure 5-1(b)). The best combinations of working base parts were used to replace the failing pieces, but as no actual spare parts were available, this process could not continue indefinitely. The best combinations of base "halves" were found by comparing signal amplitude and rates in a simple cosmic ray test using an organic scintillator read out by a standard PMT. Operating in this mode, the detector was able to limp along during development of the new GIM.

Chapter 3

The Gamma Intensity Monitor Revised

3.1 Motivations for Change

Early in the summer of 2007 it was determined that the original Gamma Intensity Monitor was not operating properly and was disassembled to assess the extent of its problems. At this time, the photomultiplier bases were the most obvious and immediate problem. They were constructed in a non-standard way by attaching two circuit boards together with delicate pin header and copious amounts of epoxy as shown in Figure 3-1. Generic prototyping board was used instead of having specialized PCB made, and normal wire was used in places where the limitation of prototyping board could not be worked around. A certain fraction of these bases worked, but each had its own quirks and failure modes. No spares existed to replace the failing components, so the GIM was only able to operate in a scaled-down configuration of its original design.

Another problem that was not understood was an anomalous hum that existed on several of the signal lines that was believed to arise from RF noise in the experimental area leaking into the GIM enclosure and readout electronics. A side effect of the open design of the original enclosure was that it was also not light tight, and for a period of time it was covered by a cardboard box to temporary keep stray light from triggering

Figure 3-1: Representative example of original base construction showing pin header used to connect base parts

the detector.

After opening the original GIM, several more problems were discovered. The old structure that originally pressed against the bases for proper optical contact at the junction between the silicon pads and the PMT's and crystals consisted of an aluminum plate covered in foam that pushed on the pieces of the old base circuit boards connected to the PMT sockets. Four bolts at the rear of the GIM pushed on this plate at its corners but could not provide pressure evenly across the sixteen tubes. This allowed for air bubbles to form between the silicone pads and the PMT photocathodes and the PbF_2 crystals, serving for points of internal reflection and loss of signal.

It was later discovered after new bases were made that most of the original bases and PMT's did not operate at their expected efficiencies even if they appeared to work properly at low rates. Many of the solder joints on the original bases were poorly made and provided additional capacitances that could slow down the time constants of some of the circuits.

Due to the extent of the problems in the original GIM, it was not possible to construct a fully working detector out of the original components. To fix the problem inherent to the old GIM. A new GIM had to be built mostly from scratch. The enclosure was redesigned and a modified holding structures was added, new bases

were made and assembled, new PMT's were acquired, and all of these components were tested and calibrated. In redesigning these components, the main themes of the original design were preserved but great care was taken to ensure that everything was robust and well thought out. A schematic of the final design is shown in Figure 3-2.

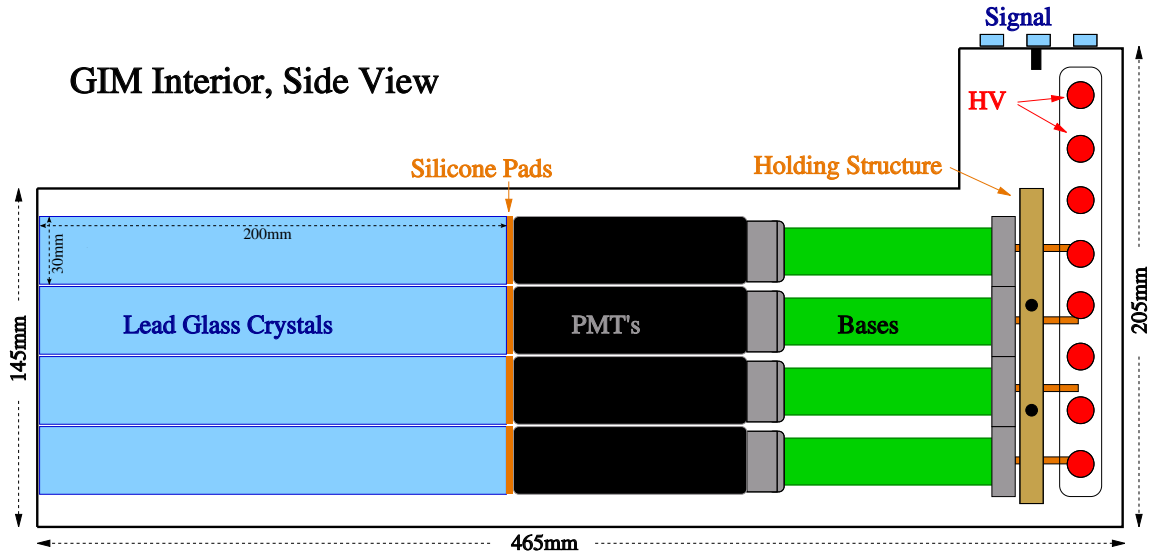

Figure 3-2: Cartoon Representation of the New Gamma Intensity Monitor

3.2 New Enclosure

The enclosure that houses the main detector components was redesigned to isolate the detector from RF noise and ambient light in the experimental hall, to isolate the grounds of the high voltage and signal lines from the enclosure, and to provide a robust support structure for maintaining good optical contact between the crystals and PMT's. The current design also allows for the detector to rest on the same pedestal as the original GIM and for the signal paths out of the detector to be completely sealed by using pass-through connectors. The enclosure itself is fabricated of 10mm thick aluminum plates whose surface is effectively continuous except for the holes for the signal and high voltage connectors which are electrically isolated from the enclosure by plastic spacers.

The front of the box through which γ's enter is covered by an opaque plastic

block bolted to the aluminum frame. A thin aluminum sheet is placed between the plastic front piece and the lead fluoride scintillators to provides RF shielding from the forward direction. Some degree of electron-positron pair production will occur in this region, but this does not present a problem. The most important change in the enclosure is the addition of a holding structure that individually pushes on each of the PMT-base combinations through 16 set screws to ensure that air bubbles do not form on the interfaces of the silicone pads and the PMT's or crystals.

3.3 Signal Processing

All of the signal processing for the GIM is done with standard NIM and CAMAC electronics in a rack below the detector with TDC and ADC analyses done on a larger rack shared with other detectors. The basic schematic of the local signal processing is depicted in Figure 3-3. All of the electronics and the GIM rack itself are on the same ground as the other main readout electronics in the experimental hall to avoid ground loops. The high voltage supply used is a LeCroy 32-channel, network controlled high voltage supply. Each base voltage can be set independently via a web interface with nominal operating voltages for the GIM bases around 1200 V.

The signals that come out of the GIM are immediately split between an analog and a digital branch. The analog branch exists to record the total intensity of the waveforms by using an Analog to Digital Converter (ADC) but had not yet been implemented in the summer of 2007. It is planned to use these signals to calibrate the supplied base voltages to equalize output signals across all channels and to verify that the signal amplitudes and discriminator thresholds remain stable during beamtime periods. It was perceived that signal attenuation between the GIM rack and the ADC would be problematic, so low attenuation AIRCOM PLUS cables (with roughly one fifth the attenuation of RG58) were run between the two areas. It is planned that the analog branch will begin operation in the summer of 2008.

The digital branch is used to make a time stamp of each event that is recorded at the GIM using a multi-hit Time to Digital Converters (mTDC) capable or recording

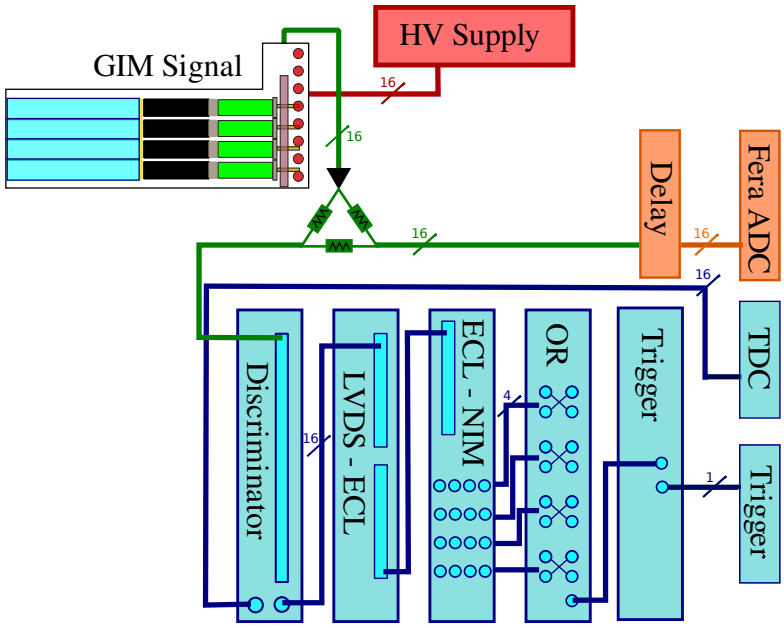

Figure 3-3: Diagram of GIM readout electronics

up to 16 hits within a one microsecond window per channel. The timing value for an event is determined at the TDC in comparison to a reference signal generated by the experimental trigger. Knowing the exact timing of γ's at the GIM is used for determining the total flux of γ's through the target (which is used for determining the total cross section) and the photon definition probability at the tagger.

To prepare the output signals from the GIM for the TDC, a very fast, 16 channel discriminator is used. The thresholds used for each channel can be programed by RS-485 protocol; their values depend on the inherent gain of each of the PMT+base combinations as originally determined by the method described in Section 6.5. The outputs of the discriminator are sent in two directions. Half go directly to the TDC where statistics are recorded on the timing of events for each channel individually; a logical OR is made of the other half as shown in Figure 3-3 to be used as trigger signal for the GIM.

Chapter 4

Ĉerenkov Radiating Crystals

4.1 Conceptual Basis

For the Gamma Intensity monitor to accurately count the high energy photons that pass through the main detectors, the energy in the γ's has to be shifted to a range that can easily be observed by normal photomultiplier tubes. This is done by passing the photon beam into an array of lead fluoride (PbF_2) crystals in which the γ's electron-positron pair produce; these paired leptons are highly relativistic and Ĉerenkov radiate in the visible to near ultraviolet regime. The cross sections for relevant scattering processes in lead fluoride are shown in Figure 4-2. The pair production cross section is extraordinarily high for scattering off the nuclear field in the energy range we are considering with values of roughly $.105\frac{cm^2}{g}$.

The lead glass crystals are optically transparent above 400 nm. The Ĉerenkov effect is enhanced by the high index of refraction of lead glass with a value of around 1.7[5]. Electron range data for lead fluoride is shown in Figure 4-3; it is important to note that many of the pair produced electrons will not be confined to the crystal in which they originated. This is actually useful in determining where the center of energy deposition is within the crystal as sub crystal level accuracy can often be acquired when a large number of crystals are involved.

The crystals used in this detector are rectangular prisms 3cm by 3cm by 20cm as shown in Figure 4-1 The length of the crystals was chosen to optimize the percent-

Figure 4-1: Stack of PbF_2 crystals before final GIM assembly

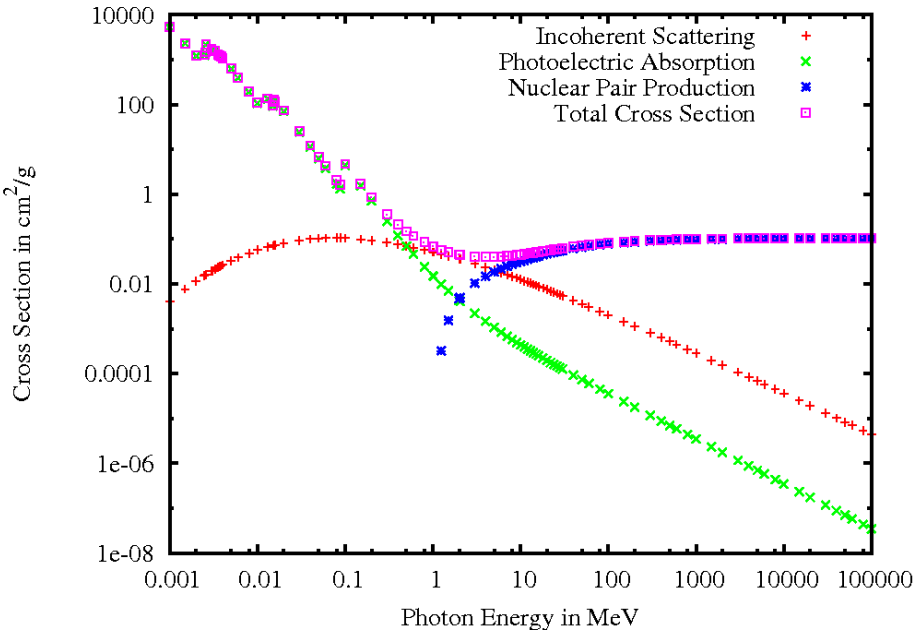

Figure 4-2: Cross Section of γ's incident upon PbF_2 [4]

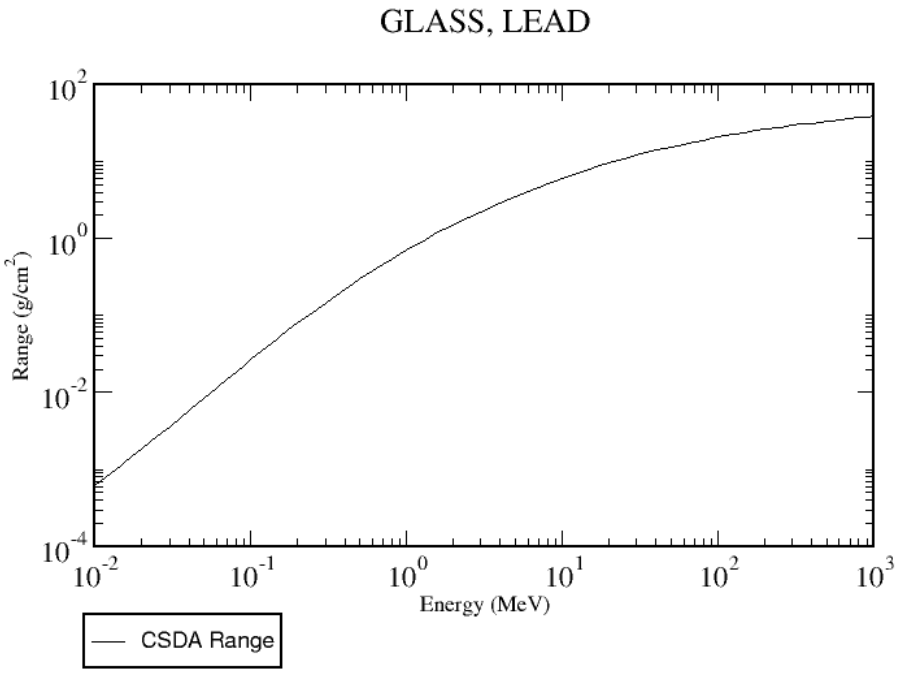

Figure 4-3: Electron Range in Lead Fluoride [4]

age of photons that would pair produce within the length of the crystals (they are 18 radiation lengths long) while maintaining low decay time for the Ĉerenkov light produced within the crystals. Using the cross section data shown in Figure 4-2, the total cross section of the crystal is calculated as in Equation 4.1 with a miss rate of $\approx 3 \times 10^{-8}$ The decay time (a measure of how long it takes to extract light from the specimen) for the crystal used is roughly 10 ns, this is expected as light traverses the length of the crystal in around 1 nanosecond and is sufficiently short to allow photon counting in the MHz regime with low signal overlap.

$$I(z) = I(0)e^{\Omega \times \rho \times L}, \quad \frac{I(20cm)}{I(0)} = e^{-0.105 \frac{cm^2}{g} \times 8.24 \frac{g}{cm^3} \times 20cm} \approx 3 \times 10^{-8} \tag{4.1}$$

4.2 Optical Contact and Isolation

To ensure robust optical contact between the crystals and the photomultiplier tubes, silicone pads as suggested by [5] are used as spacers. Pressure is applied from the rear of the photomultiplier tubes to keep air bubbles from forming on the interfaces on either side of these pad through an array of set screws (one for each channel) that sit at the rear of the detector.

To increase the amount of Ĉerenkov light detected at the PMT and reduced the amount of cross-talk between channels, the crystals are longitudinally wrapped in a thin layer of aluminized mylar. It has been shown that certain wrappings can improve the light yield by around 10 percent [5]; aluminized mylar is used as it is thin and highly reflective. Optically isolating each of the channels is helpful when determing the center of mass of energy deposition within the detector.

Chapter 5

Photomultiplier Tubes

5.1 Specifications

The Ĉerenkov photons produced in the lead glass crystals are measured with Photonis model XP2900 $1\frac{1}{8}$inch (29 mm) photomultiplier tubes covering 73% of the surface area of the crystals. They have a spectral range of 270 to 650 nanometers with an optimal quantum efficiency at 420 nanometers (3eV)[10] which is ideal for this application. The tubes have 10 dynodes optimized for high count rate applications and the photocathode is made of a bi-alkali metal that minimizes dark currents. To properly position the tubes behind the stack of lead glass crystals,they are suspended in a block of paper-formed silicone with cylindrical holes the appropriate size for the tubes as shown in Figure 5-1(a). This setup allows for the tubes to slide along the direction of the photon beam so that pressure can be applied through each of the tubes individually to ensure proper optical contact to the lead glass crystals.

5.2 MCA Tests and New PMT's

To evaluate the performance of the original photomultipliers, each of the tubes was tested with a standard light source and the same base. The light source was provided by irradiating a 5mm thick plastic scintillator with .546 MeV electrons from ^{90}Sr. Each base was provided with 1200V net voltage, and these tests were performed in a

(a) PMT's photocathodes during assembly

Front View

1	2	3	4
5	6	7	8
9	10	11	12
13	14	15	16

(b) Channel Numbering Scheme

Figure 5-1: Front view of PMT's and associated numbering scheme

light tight, RF shielded box. The scintillator and tube were held snugly in a plastic block machined for this purpose as shown in Figure 5-2 to ensure consistent alignment of the tube and scintillating block. Signals were binned into a histogram based on time integrated voltage of the peaks with a Multi-Channel Analyzer (MCA)

The surprising result of these tests was that the PMT's used in the original GIM fell into three groups based on their output signals. Figure 5-3 shows representative spectra for each of these groups. Four of the tubes were is the left-most group where no clear signal peak can be distinguished from the dark currents (the lowest most energy peaks on the left characteristic of all PMT's); eight were in the middle group where a signal peak is barely visible, and four were in the right-most group where the signal peak is well defined.

After it was realized that the original PMT's were not sufficient for the new GIM, new photomultipliers were acquired from the University of Mainz, and additional tests were done to calibrate their signal output to a standard level. This testing procedure was similar to the earlier PMT tests used to verify their amplification levels

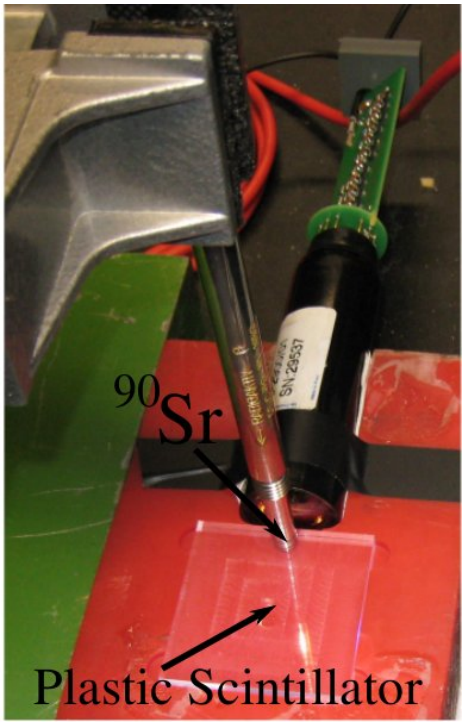

Figure 5-2: Apparatus for evaluating PMT performance

except that a second scintillator read out by another PMT was placed below the main scintillator and used as a trigger to ensure that only signals from minimally ionizing electrons were analyzed. The signals from the tubes being tested were averaged over 2^8 pulses in an oscilloscope, and the supply voltages to the bases were adjusted until the average response for all of the base/PMT pairs were roughly equal in value (12mV). Results results from this test are tabulated in Appendix E.2.

5.3 Comment on Damaged Tubes

It is unclear when the original tubes became damaged, but it is my opinion that gamma's unscattered in the crystals or energetic electrons are responsible. The flux at the photocathodes should be 10^{-8} of the total flux from Equation 4.1, but some kind of electromagnetic shower could easily damage the PMT's. The main beam of γ's has a width of several centimeters at the GIM, so the crystals in positions (as described in Figure 5-1(b)) 6, 7, 10, and 11 see the highest flux of γ's. Positions

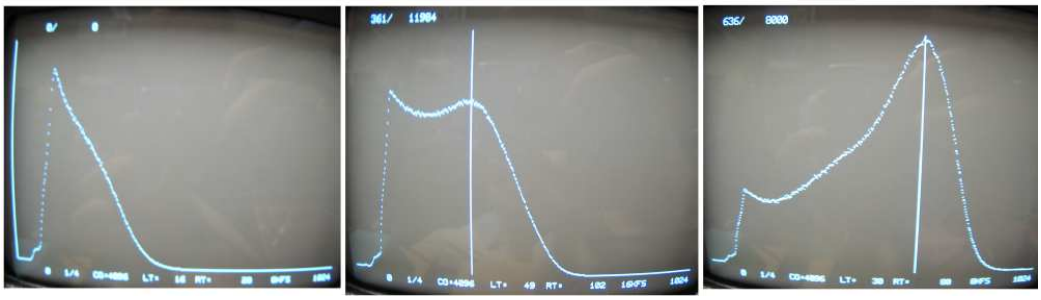

Figure 5-3: Comparison of MCA spectra seen from original PMT's

2, 3, 5, 8, 9, 12, 14, 15 would receive lower rates resulting in medium damage, and the tubes behind crystals 1, 4, 13, 16 would receive the lowest flux of γ's and the lowest damage. The performance of the new PMT's will likely decrease with time and should be monitored for signs of degradation.

Chapter 6

High Rate Photomultiplier Bases

6.1 History

The largest task in rebuilding the GIM was building new photomultipler bases that would work reliably at count rates up to 10MHz. Commercially available bases are not designed for count rates this high. Luckily, bases meeting our specifications had already been designed for use in the detectors at MAMI and in the COMPASS detector at CERN. To use these bases in our detector, the physical design of the circuit boards was slightly modified as pressure was to be applied through them to ensure uniform optical contact between the photomultipliers and the crystals. The only remaining task was to have these bases printed, assembled, and tested as quickly as possible so that the detector could resume operation.

The purpose of the bases is to serve as a voltage division chain and as a signal conduit for the PMT. They are constructed in two parts: a round board that contains the capacitors closest to the dynodes and holds the socket (used for connecting to the leads on the PMT) and a rectangular board which contains the voltage dividing resistor/transistor network. The circuit boards are laid out to reduce the probability of arcing between adjacent components and pads; the average spacing between pads is about 1.75mm which gives a breakdown voltage (based on the breakdown voltage of air at 3 million volts per meter) around 5000V, a value much higher than these boards will experience. To further reduced this risk and increase the mechanical strength of

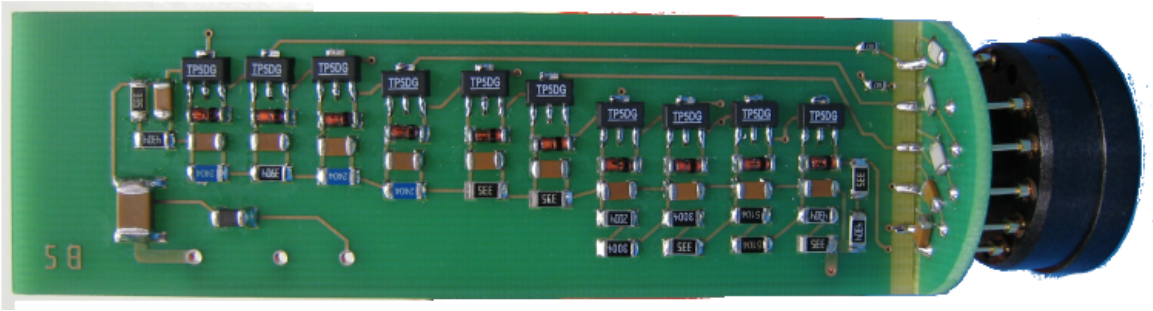

Figure 6-1: Completed circuit board with Socket

the system, the boards are covered in a layer of high-strength epoxy; this is standard practice in high voltage applications.

Due to size constraints, the surface mount pads are roughly the same size as their associated components. This makes soldering problematic. As solder often has to flow under components to make a connection, the high-frequency transmission properties at these places is different from normal joints. No anomalous properties were observed in the bases at high count rates, so it assumed that this does not present a problem.

An example of a completed board before the socket, HV and signal cables, and the end cap have been attached is shown in Figure 6.1; a parts inventory and circuit diagrams are listed in Appendix C.

6.2 Dynode Tests

As a first test of the bases after the PCB's were populated, the voltages distribution network was verified by measuring the supplied voltage on each of the dynode channels with 300V input voltage to the base. These were compared to similar tests performed at Mainz on their PMT bases (after which these are designed). The comparison values from the Mainz bases were taken as the mode of tests run on 14 of their bases and are consistent with the values measured on our bases. A summary of the data from these tests is listed in Table E.1.

Through verification of the voltage distribution chain, the average potential difference seen between adjacent dynodes was determined and compared to the expected

Figure 6-2: Voltage Differences Between Dynodes @300V

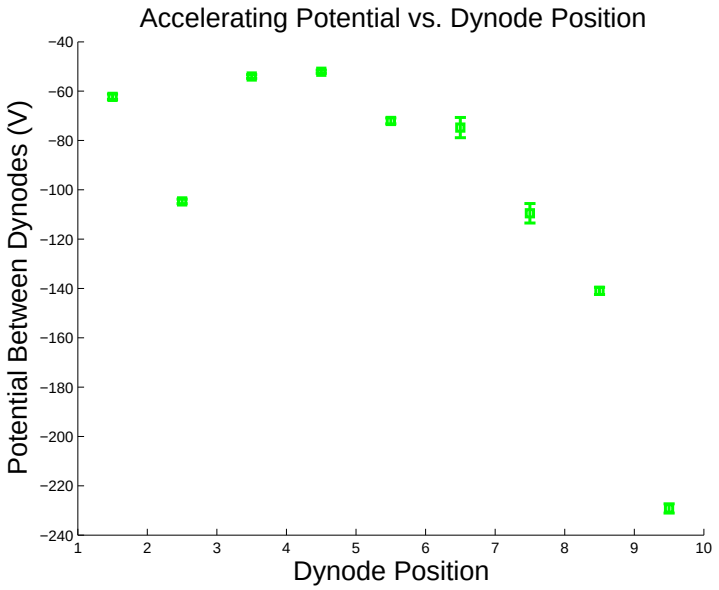

values. Standard configurations exist for the voltage pattern along an amplification chain–a linear relation gives greatest amplification and largest dark current whereas an exponential pattern gives good timing and low noise. To determine the optimal configuration for these photomultipliers, the University of Mainz connected each of the dynode channels to a HV source and examined thousands of voltage combinations to discover the configuration that optimized both timing and amplification at high count rates. The relative voltage difference between adjacent dynodes for the Mainz base are listed in Table 6.1. Figure 6-2 shows the data for the new GIM bases as a function of dynode number.

Table 6.1: Optimal relative voltage differences between dynode for good timing and linearity of gain (A is anode which is connected to ground)

Dynode Position	1-2	2-3	3-4	4-5	5-6	6-7	7-8	8-9	9-10	10-A
Photonis[10]	1	1.5	1	1.25	1.25	1.5	2.25	2.25	2.5	3
Mainz Optimal	1	1.65	1.0	1.0	1.4	1.4	2.1	2.6	4.3	3.1
GIM Base	1	1.57	0.9	0.9	1.4	1.4	1.9	2.5	4.0	2.8

To ensure that the bases behave linearly in response to input voltage, the voltages supplied to each of the dynodes was measured at a variety of input voltages. The

data collected (from Base 2) is shown in Figure 6-3; the lines plotted in graph are linear fits to data; errors in the points were not estimated. It is assumed that all other bases act similarly.

Figure 6-3: Linearity of Dynode Voltage Scaling vs. Input Voltage

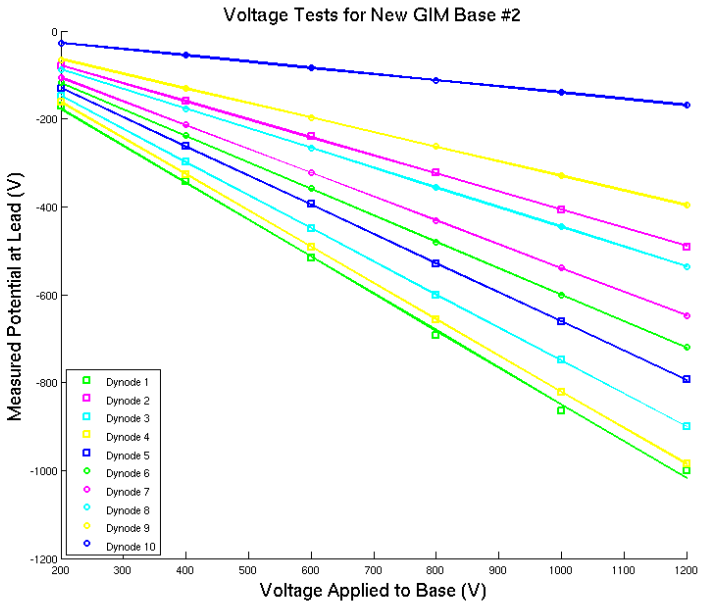

6.3 Output Signals

Since the voltage networks worked as expected, a combination of PMT+base was used to test signal quality by looking at cosmic rays. A comparison of new signals to that of an old GIM base and a Mainz base read out on an oscilloscope are shown in Figure 6-4. All test were done with a lead fluoride (PbF_2) crystal and Photonis XP2900 photomultiplier optically coupled through a silicone pad. Scale on oscilloscope is 5mV and 10ns per division; the displayed signals are averages of the last 256 counted signals. The resulting signal from the new base is much cleaner than that produced by the old bases and provides good amplification.

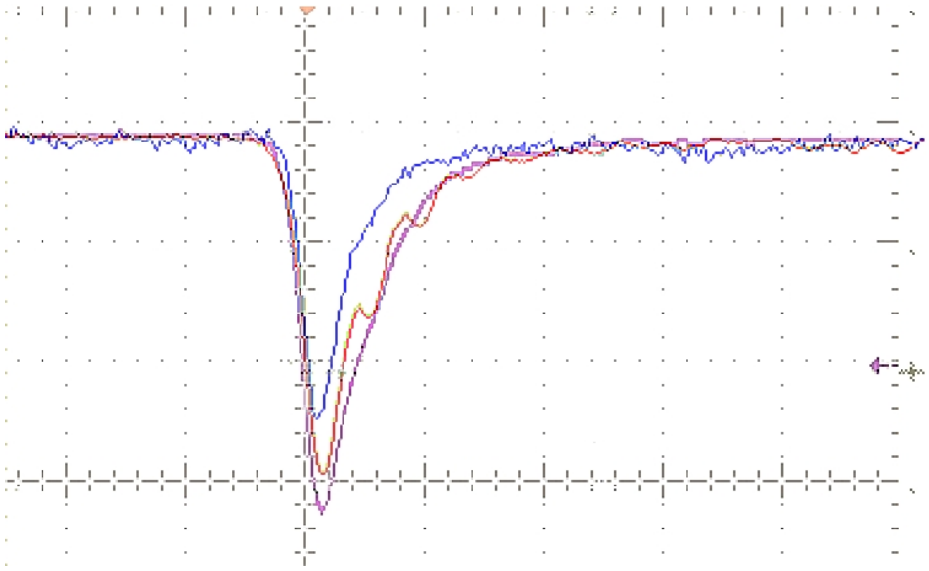

Figure 6-4: Signal comparison overlay: blue is Mainz base, red is old GIM base, violet is new GIM base

6.4 Comparison of New Bases

Knowing that the voltage network works as expected, we next tested the bases under actual operating conditions using a setup similar to the one described in Section 5.2. The relative orientations of the Strontium source, plastic scintillator, and photomultiplier tube were held constant with clamps and tape allowing the bases to be exchanged without modifying the setup as shown in Figure 6-5. The voltage supplied to bases was 1200V in all tests, and the output signals were amplified by roughly a factor 25 to accommodate the range of the MCA used to bin the data. Base 6 (serial number 28161) was tested first and last to ensure that systematic drift was not effecting the results of the test.

A screen shot of a typical MCA analysis for the new GIM bases is shown in Figure 6-6(a). Most of the bases behaved effectively identically with good signal to dark current separation. For comparison, the same test was run with one of the original bases at 1200, 1250, and 1300 V; the analyzed signals are shown in Figure 6-7. Notice that the signal to dark current ratio is low and that the signal peak is only barely distinct from the dark current background when operated at 1300V.

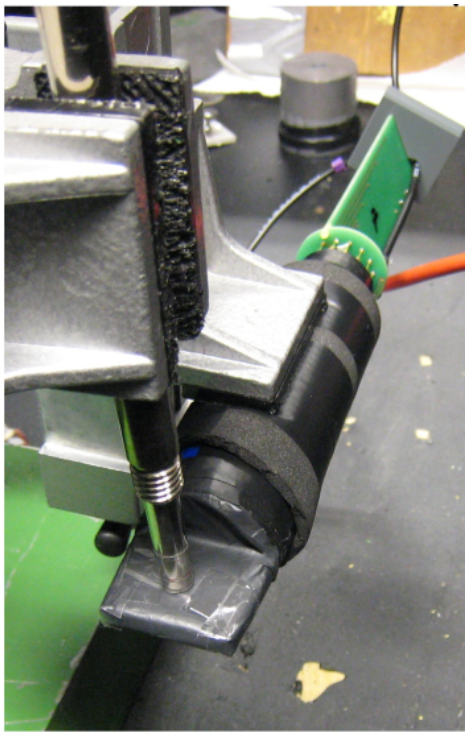

Figure 6-5: Apparatus used for testing base performance

The signal amplitude from the photomultiplier+base setup we use responds linearly to change in applied voltage. This was determined using the apparatus described above by varying applied voltage instead of base. Figure 6-6(b) shows the location of the peak of the MCA binned spectrum as a function of applied voltage. The scaling is exceptionally linear once a threshold of around 1150 V is reached; a linear fit is shown to the last 6 data points in this region.

6.5 Final Calibration

To prepare the PMT+base pairs for use in their final configuration, their supply voltages were adjusted to equalize their output to a standard value. The bases with naturally higher gain were paired with the tubes with naturally lower gain to make this process easier. The setup used was the same as in the PMT testing using a secondary detector as a trigger as described in Section 5.2. Signals were averaged in an oscilloscope so that voltages could be adjusted easily in real time. Better optimization

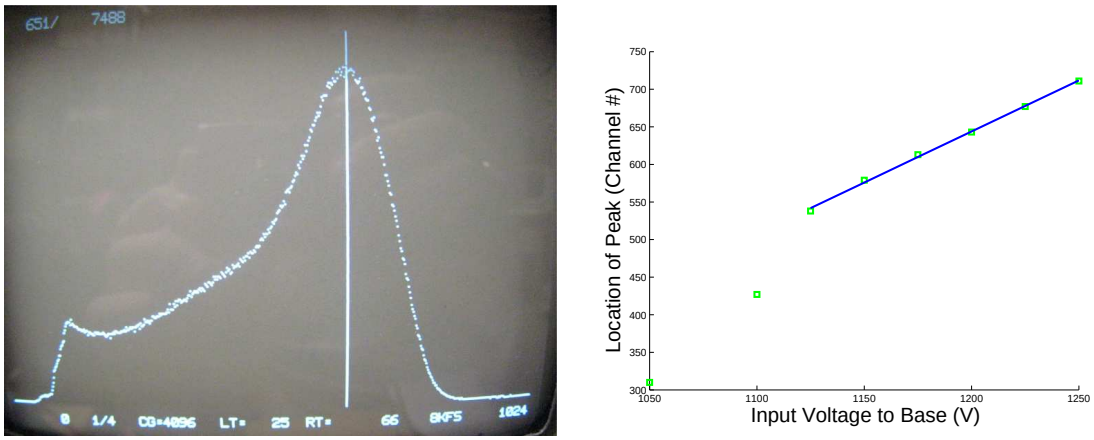

(a) Sample MCA spectrum from new GIM base

(b) Peak scaling at different input voltages

Figure 6-6: MCA data from new GIM bases

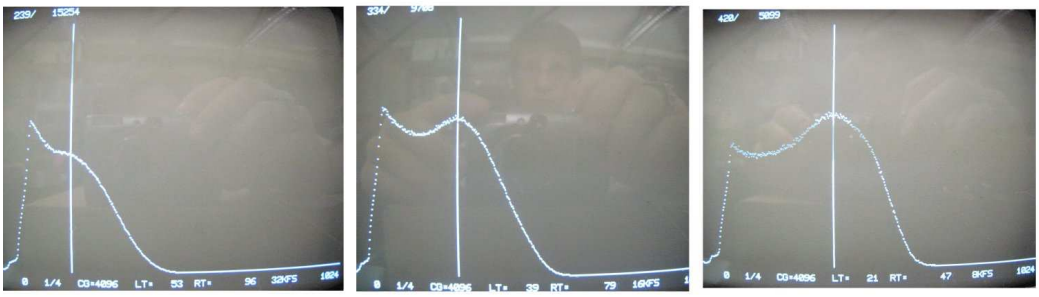

Figure 6-7: Output signals from original bases at 1200, 1250, and 1300 V as binned by the MCA

of the supply voltage for each channel will have to be done in the experimental area with cosmic rays and later with beam photons.

Chapter 7

Initial Findings and Conclusions

7.1 Initial Data

The final assembly of the new GIM installed in the experimental area is shown in Figure 7.1. Voltage levels of the PMT bases were set at the values determined in Section 6.5 and the first in situ tests were performed with a high rate gamma beam. Signals from each GIM channel and a logical OR of all channels were sent to an mTDC's where timing data was recorded for each event.

As a fun test of the detector in its final configuration, signals from each of the four vertical columns of four crystals (such as channels 2, 6, 10, and 14) were sent to an oscilloscope with the bottom-most channel used as a trigger (one could use the top channel, but sometimes the incident particle will stop before it reaches the lowest crystal). Cosmic rays naturally pass through the detector, and one observes each of the four channels firing one after the other separated by fractions of a nanosecond showing that good relative timing exists between the channels.

Using the mTDC, the total count rate at the GIM from the main beam was examined as a function of discriminator threshold level. The plot shown in Figure 7-2 was constructed to show this variation based on a logical OR of the signal channels. Naively, one would expect this graph should have the same general shape as the energy spectrum of the incoming gamma's, which for bremsstrahlung has an exponential suppression with increasing energy. This is consistent with observation but does not

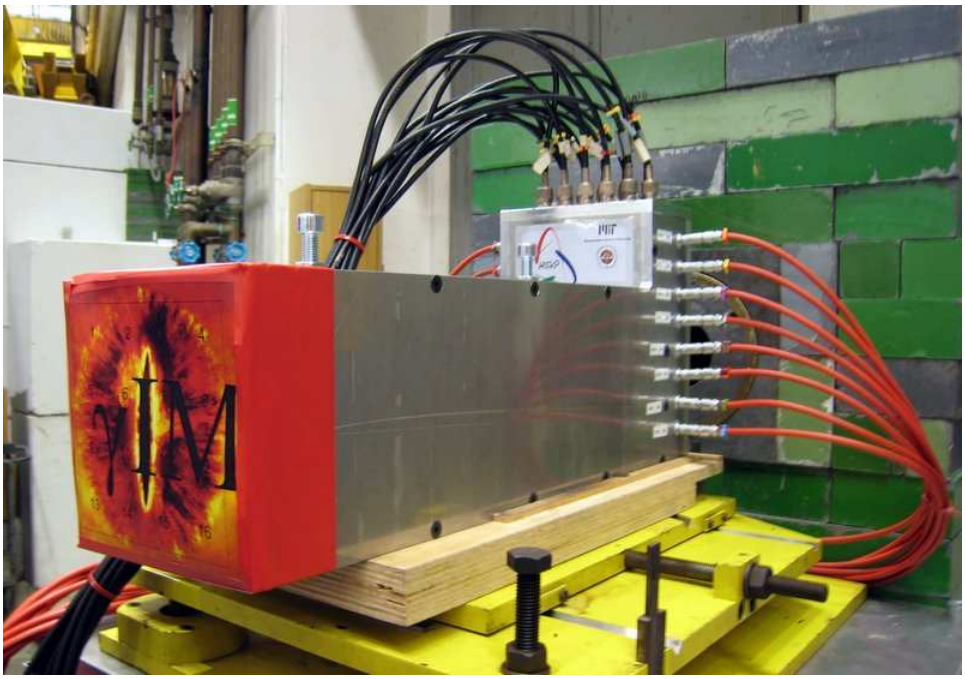

Figure 7-1: GIM installed in the experimental area

rigorously prove that a usable correlation exists between gamma energy and signal amplitude.

The total count rate in each channel with standard discriminator levels is recorded by the mTDC and displayed graphically in Figure 7-3(a); each square represents events in its respective crystal as shown in Figure 5-1(b). Count rates are higher in the central crystals as the detector is aligned such that the center of the beam should passes through the center of the detector. To verify that this alignment is true, mTDC information from each channel is used to determine the centroid of energy deposition within a given GIM event. A GIM event is defined as a set number of signals adjacent in time (for this example 20 hits is assumed); the geometric mean of the positions of the crystals in which these signals originated gives the γ's decay location. To ensure that all of these hits were from the same γ, only hits that occur within 35 nanoseconds of the middle hit are counted. This data from 110,000 events is plotted in Figure 7-3(b) with a beam center determined to be 0.06773 cm horizontally and 0.4274 cm vertically from the center of the detector. The distribution had a horizontal RMS width of 0.6895 cm and vertical width of .6515 cm. After viewing in the count rates

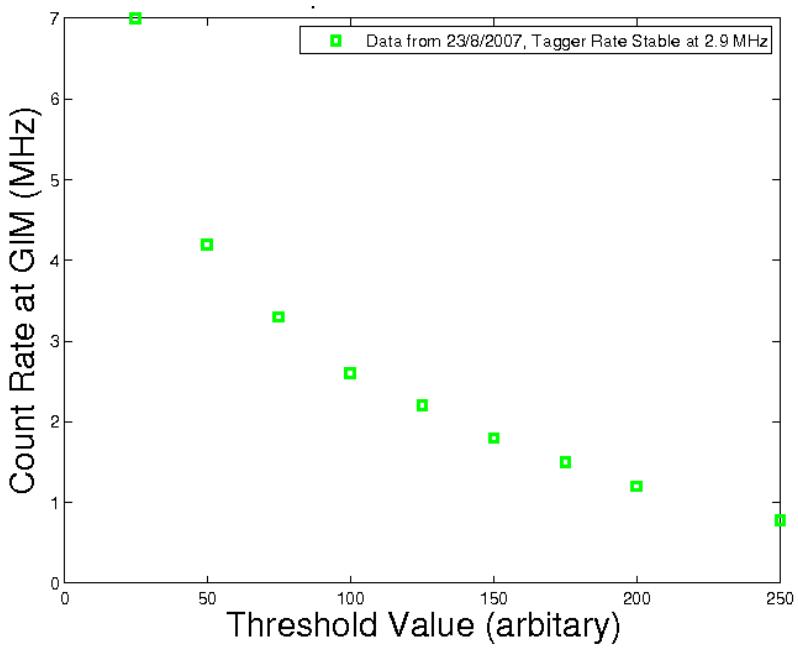

Figure 7-2: Count rate dependence on threshold value

observed in Figure 7-3(a), it was decided to discontinue use of channels 1, 4 13, and 16 as count rates in these channels were exceptionally low. The bases from these channels have been reserved as spares should any of the others fail.

7.2 Conclusions

The new Gamma Intensity Monitor was redesigned and rebuilt to resolve the issues inherent to the original detectors. It has been shown to shield ambient RF noise, to ensure even optical contact between the radiating crystals and the PMT's, and to operate robustly with consistent amplification at high count rates. The detector's form factor is compact and should be easily adaptable for future experiments. Its design and implementation were carefully thought out and rigorously tested. With this detector, the Crystal-Barrel-Collaboration will be able to further their exploration of the baryon spectrum and hopefully discover new resonances and their total cross sections.

May the Gamma Intensity Monitor live a long and fruitful life!

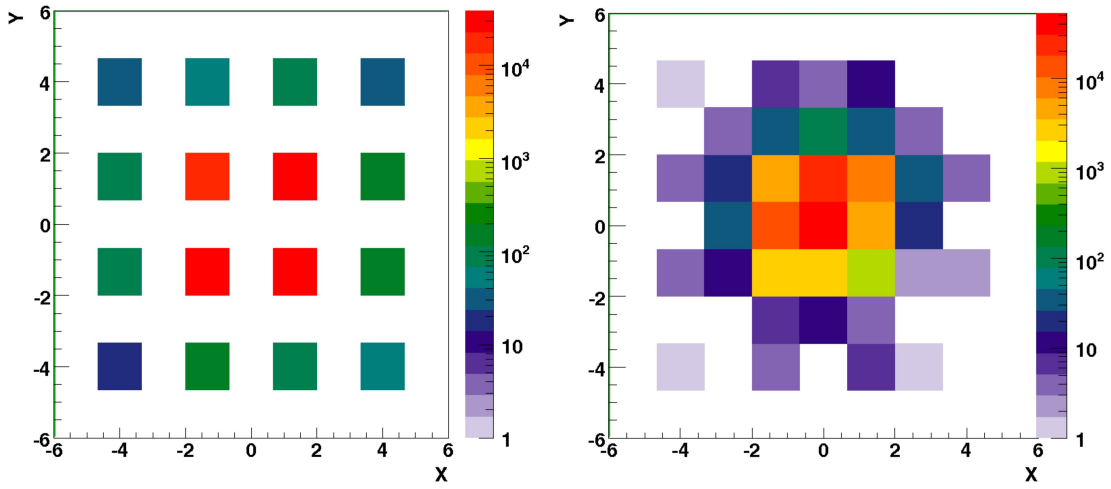

(a) Count rates by channel number

(b) Localization of beam positions

Figure 7-3: Initial count rates as seen at GIM (courtesy of Christoph Wendel from beamtime on 23 August 2007)

Appendix A

Glossary

As with any large project, many acronyms and abbreviations are used. What follows explains some of the most common abbreviations specific to the Crystal Barrel group.

- CHAPI: CHArged Particle Identification: this is part of the inner detector that resides in the square cavity in Crystal Barrel and is used to determine both spatial and charge information about particles passing through it; see SciFi.
- CB: The Crystal-Barrel-Detector
- CBFP: The Crystal-Barrel-Forward-Plug, like the CB but read out by high rate PMT's
- ELSA: ELectron Stretcher Accelerator, main accelerator ring for the Crystal-Barrel-Experiment
- GIM: Gamma Intensity Monitor, used to count γ's unscattered in the target
- HISKP: Helmholtz Institute für Strahlung und Kernphysik at the Universität Bonn
- SciFi: The Scintillating Fiber detector
- TAPS:Two Arm Proton Spectrometer, a slight misnomer as only one of the arms is in Bonn, the other resides at the Universität Mainz; at present a smaller version is in use called miniTAPS.

Appendix B

Detector Schematics

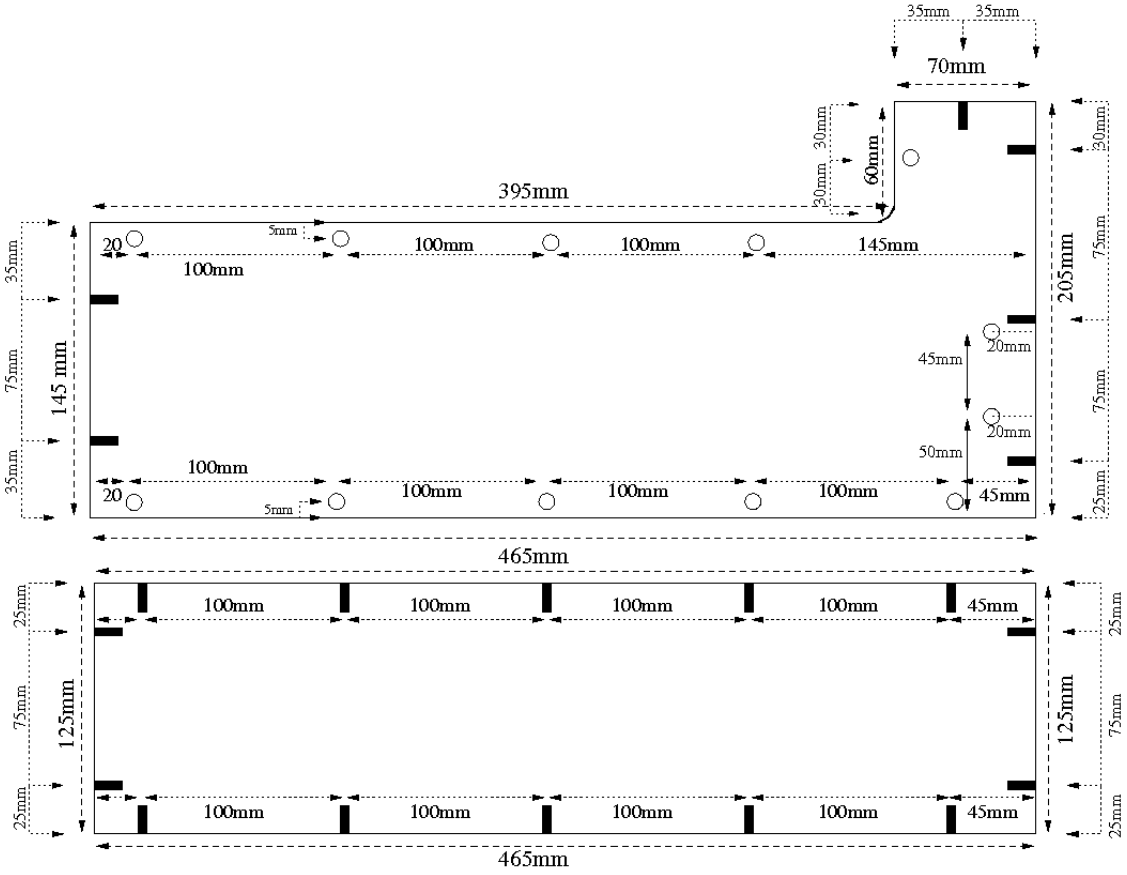

Figure B-1: Schematic of new GIM housing (side piece on top, bottom piece below)

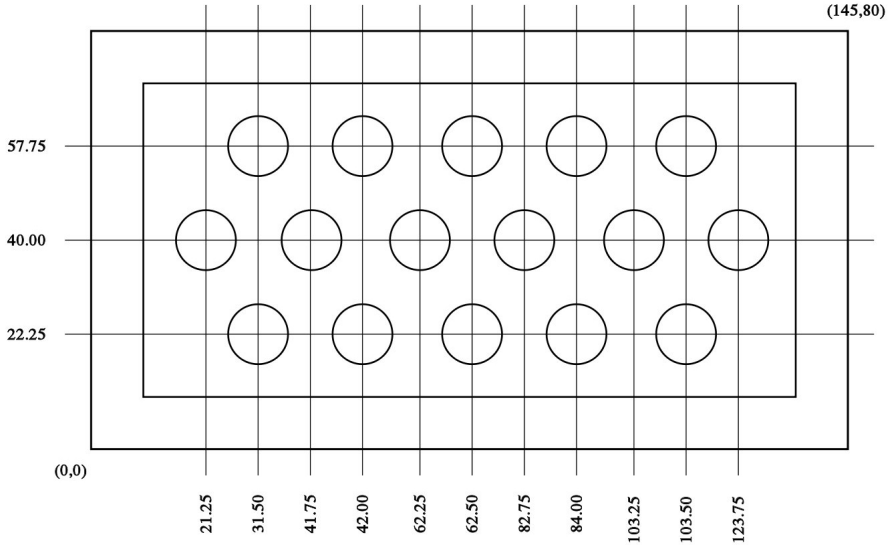

Figure B-2: Schematic of smaller top plate with signal socket holes drilled

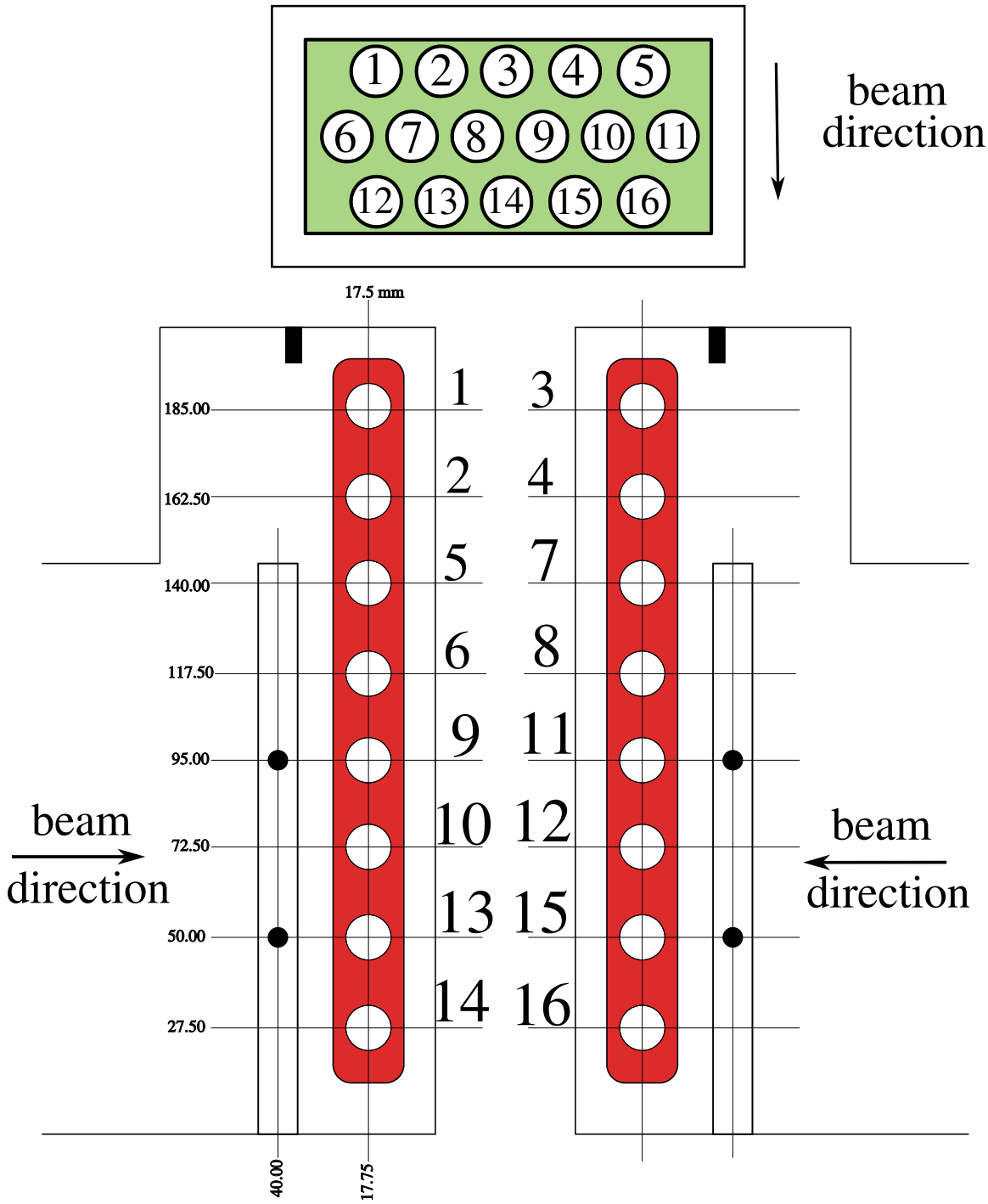

Figure B-3: Numbering scheme for HV (red) and signal (green) channels

Appendix C

Parts Inventory

C.1 Base Components

Table C.1: Parts list per base

Quantity:	Part Type:	Value:	Form Factor:
1	Resistor	$10M\Omega \pm 5\%$	1206
1	Resistor	$2M\Omega \pm 5\%$	1206
3	Resistor	$2.4M\Omega \pm 1\%$	1206
2	Resistor	$3M\Omega \pm 1\%$	1206
6	Resistor	$3.3M\Omega \pm 5\%$	1206
1	Resistor	$3.9M\Omega \pm 5\%$	1206
3	Resistor	$4.3M\Omega \pm 1\%$	1206
2	Resistor	$5.1M\Omega \pm 1\%$	1206
2	Resistor	$1k\Omega \pm 5\%$	603
1	Resistor	$470\Omega \pm 5\%$	603
12	Capacitor	4.7nF 500V	1206
1	Capacitor	1nF 3kV	1812
5	Capacitor	smallest 15-100pF 500V	1206
1	Capacitor	470pF 500V	1206
1	Capacitor	1nF 500V	1206
1	Capacitor	2.2nF 630V	1206
1	Capacitor	10nF 500V	1206
1	Capacitor	22nF 630V	1206
10	Zener Diode	BZV55 0.5W,16V	1206

Appendix D

Construction Notes

This thesis contains the information one needs to understand the GIM, but I would like to give the reader a more visual perspective on the inner workings of the GIM. It is my hope that whomever disassembles the detector in the future will find no surprises.

Important things to notice:

- In Figure D-1 the black foam protects the crystals from the housing as it is easily scratched or chipped.
- The grey caps in Figure D-3 on the ends of the bases are the surfaces on which the set screws push to keep appropriate pressure on the silicone pads.
- The arrangement of bases as shown in Figure D-3 minimizes RF noise cross talk between channels.
- Through hole sockets are used for all signal and HV connections to the GIM to make the entire detector optically isolated form
- Notice all of the wires in Figure D-6 are neatly arranged!

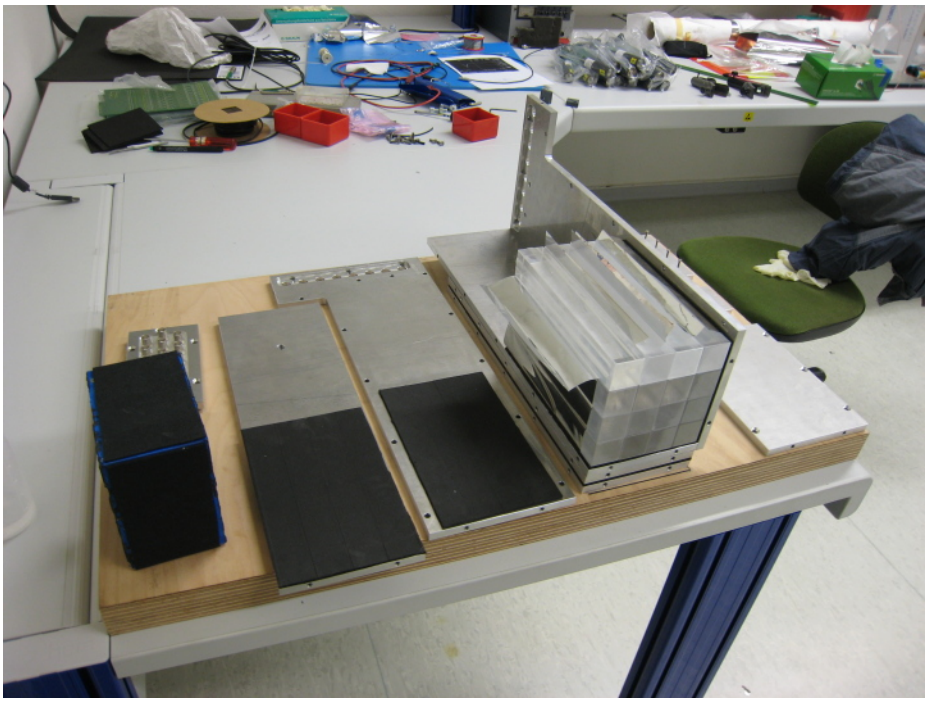

Figure D-1: Early in process of final assembly

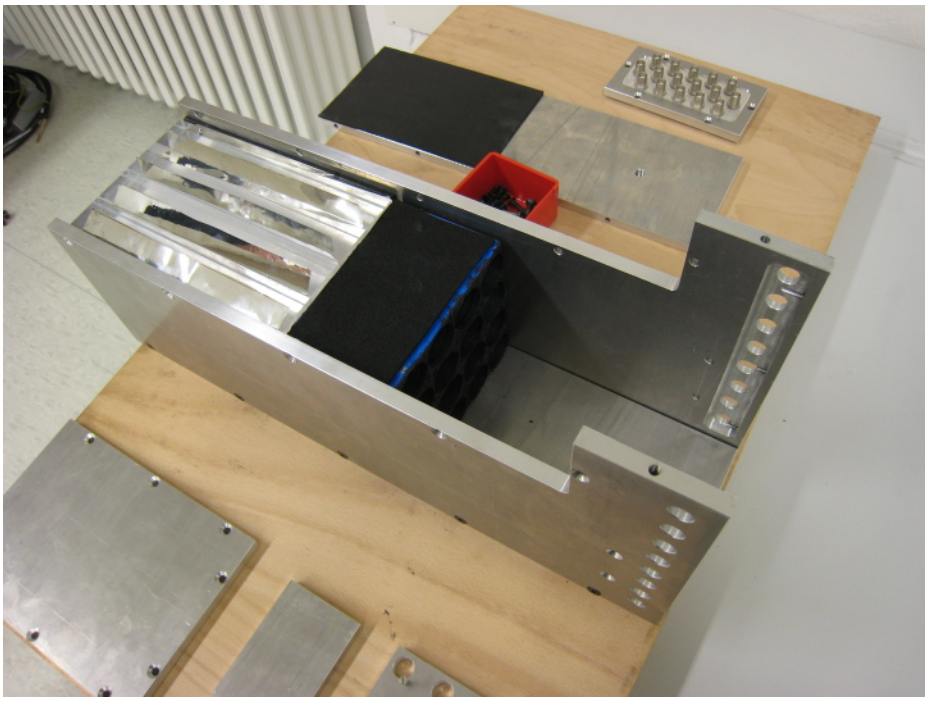

Figure D-2: Rear view showing how PMT housing sits behind crystals

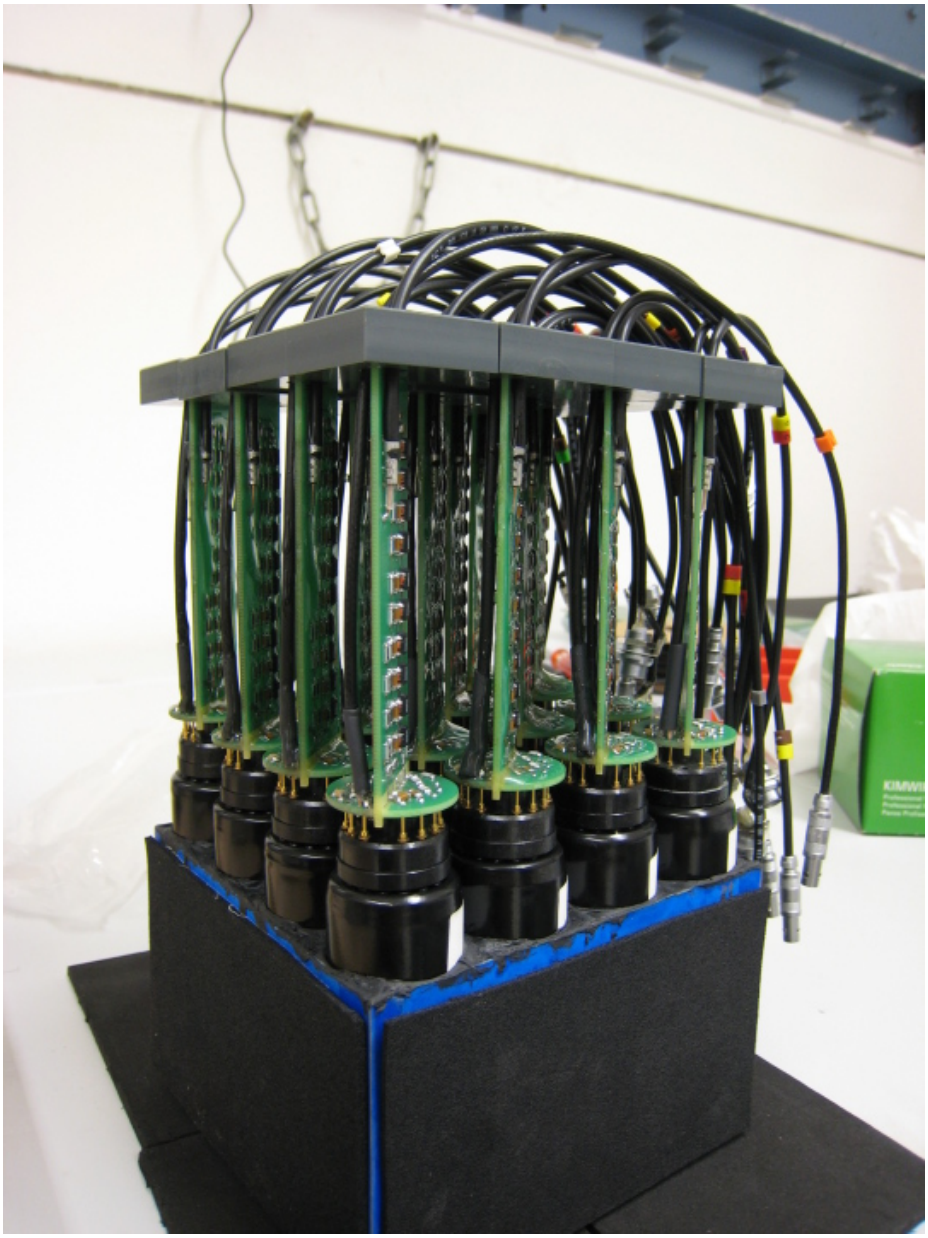

Figure D-3: Photomultipliers with their bases

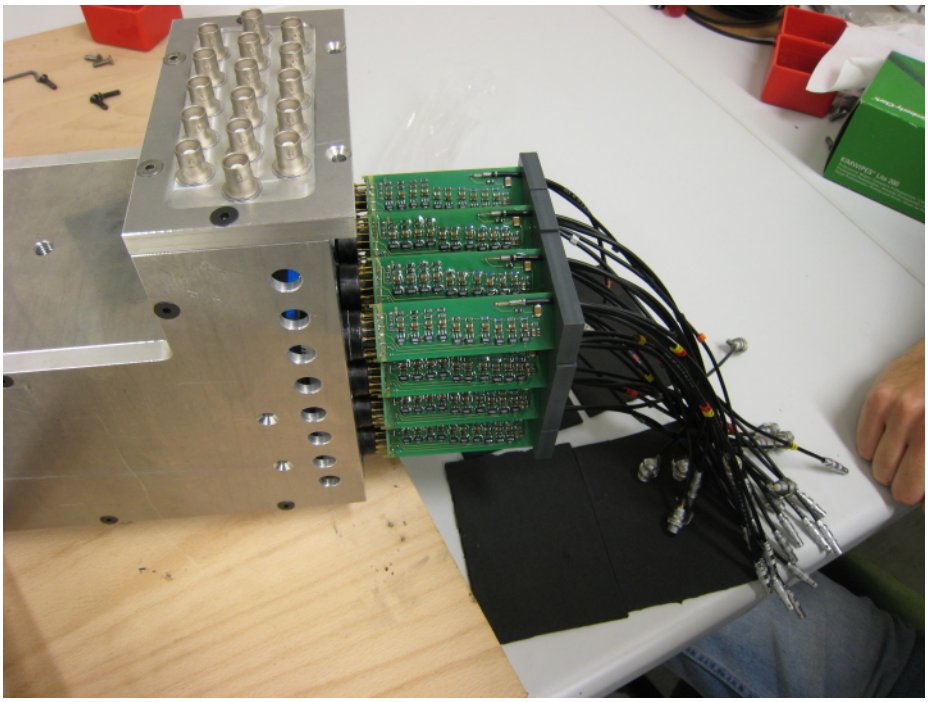

Figure D-4: Inserting PMT's into enclosure

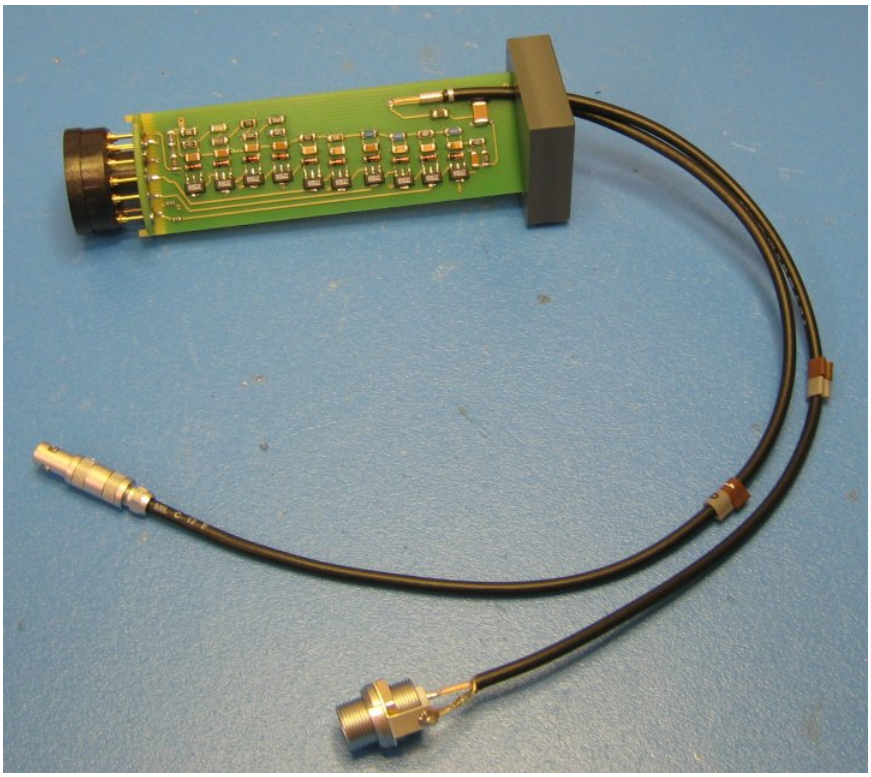

Figure D-5: Completed base with endcap, connectors, and PMT socket

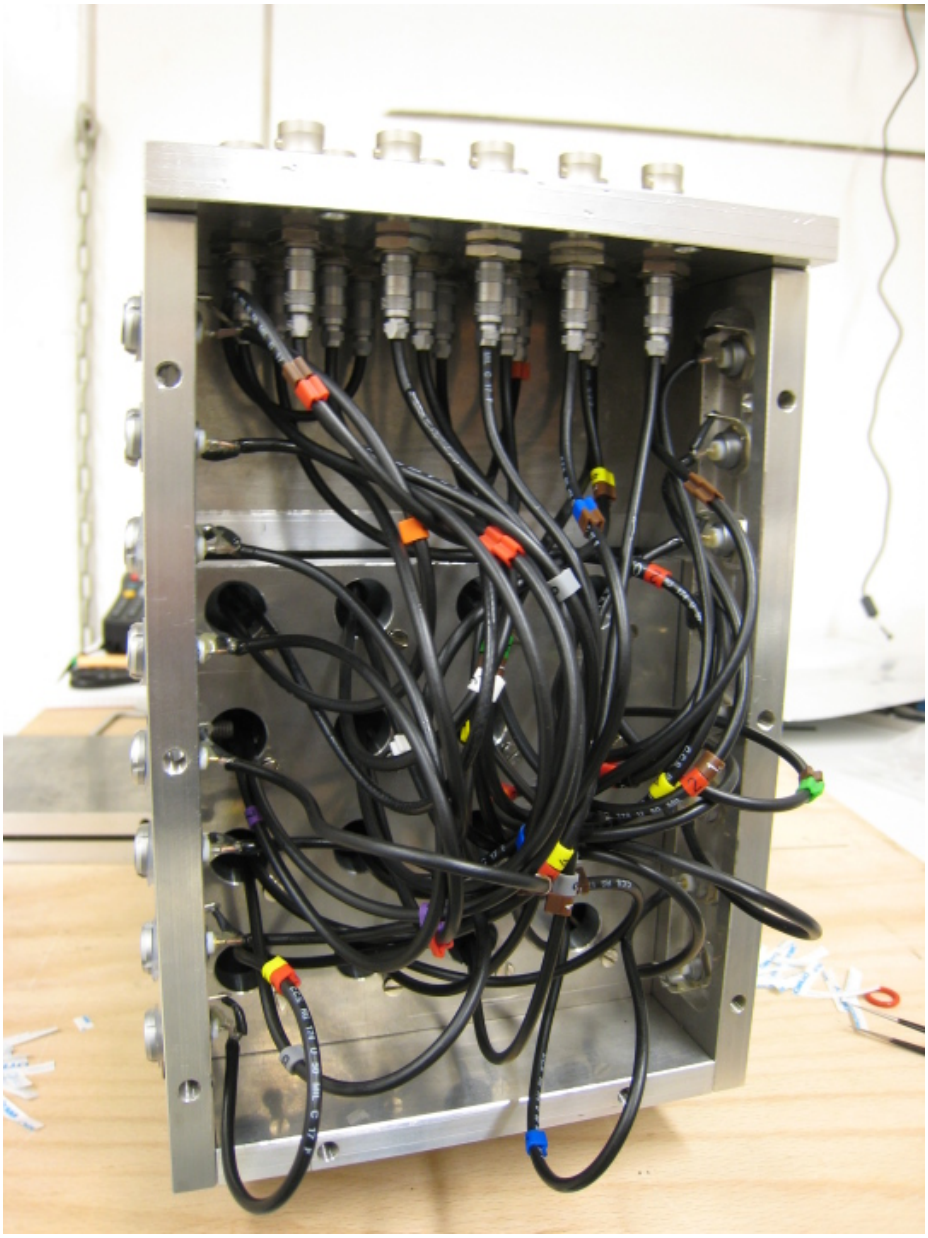

Figure D-6: Rear of detector with set screw plate and through-hole sockets installed

Appendix E

Tabulated Data from Testing Bases

Table E.1: Dynode Voltage Distribution Test at 300V (all values in -V)

Base	D1	D2	D3	D4	D5	D6	D7	D8	D9	D10	K
Mainz	258	244	222	209	196	177	158	131	96	40	??
1	296.3	295.0	292.9	291.1	274.6	262.3	235.1	194.4	143.4	60.8	120.9
2	261.5	144.3	223.0	??	196.3	177.9	159.9	132.9	97.4	41.4	119.0
3	256.8	243.6	222.0	208.5	195.4	177.5	159.5	131.8	97.1	40.0	119.6
4	256.1	242.8	221.3	208.1	194.9	177.0	159.0	131.4	96.9	40.7	119.6
5	256.2	243.9	221.5	208.3	195.2	177.1	159.3	131.8	96.5	40.6	119.7
6	256.2	243.1	221.6	208.5	195.2	177.0	159.0	131.4	96.9	40.6	119.8
7	258.0	244.6	223.0	209.8	196.4	178.0	159.6	132.0	97.1	40.9	120.9
8	258.1	244.8	223.2	209.8	196.6	178.3	156.1	132.3	97.7	41.0	120.9
9	260.1	246.9	225.3	211.8	198.4	180.1	161.7	133.5	98.6	41.4	122.4
10	258.4	244.9	223.3	209.9	196.7	178.6	160.5	132.7	97.8	41.2	120.9
11	257.9	244.8	223.2	210.2	196.8	178.6	160.1	133.1	97.8	41.5	120.7
12	258.3	245.1	223.8	210.3	197.2	178.9	160.5	132.6	97.9	41.3	121.5
14	258.2	244.8	223.1	209.8	196.5	178.3	160.4	132.5	97.7	41.0	121.7
15	258.2	244.9	223.4	210.2	196.9	178.6	160.6	132.7	98.2	41.3	121.2
16	257.5	244.1	222.6	209.3	196.1	178.0	159.8	132.2	97.1	41.8	122.0
17	258.2	245.0	223.5	210.1	196.9	178.6	160.4	132.5	97.6	41.0	120.5
18	258.1	244.8	223.3	210.0	196.7	178.5	160.3	132.7	97.8	41.1	121.6
20	259.2	246.2	224.8	211.7	198.4	180.2	162.1	134.3	99.6	???	122.4
21	258.4	245.2	223.7	210.5	197.2	179.1	161.2	133.6	98.8	41.9	124.1
22	258.6	245.5	223.8	211.0	197.2	180.1	161.3	134.0	98.1	41.9	125.6

Table E.2: Final calibration of base+PMT pairs using ^{90}Sr source to equalize outputs

Channel #	Supply Voltage
1	0V
2	1200V
3	1185V
4	0V
5	1210V
6	1215V
7	1225V
8	1200V
9	1220V
10	1230V
11	1200V
12	1155V
13	0V
14	1190V
15	1180V
16	0V

Bibliography

[1] Crystal-Barrel-Collaboration. Shared Internally.

[2] G. Suft et al. A scintillating fibre detector for the Crystal Barrel experiment at ELSA. *Nuclear Instruments & Methods in Physics Research A*, 538:416–424, September 2005.

[3] J. Naumann et al. A photon tagging system for the GDH-Experiment at ELSA. *Nuclear Instruments & Methods in Physics Research A*, 498:211–219, December 2002.

[4] M.J. Berger et al. Xcom: Photon cross section database. http://physics.nist.gov/PhysRefData/Xcom/Text/XCOM.html.

[5] P. Achenbach et al. Measurements and Simulations of Ĉerenkov Light in Lead Fluoride Crystals. *Nuclear Instruments and Methods in Physics Reserach A*, 465:318–328, 2001.

[6] S. Nakamura et al. Acceleration of polarized electrons in ELSA. *Nuclear Instruments & Methods in Physics Research A*, 411:93–106, January 1998.

[7] T. Speckner et al. The GDH-Møller-Polarimeter at ELSA. *Nuclear Instruments & Methods in Physics Research A*, 519:518–531, September 2003.

[8] E. Klempt. Baryon resonances and strong QCD, 2002.

[9] Michael Konrad. Ortssensitiver Detektor für hochenergetische Photonen bei höchsten Raten. Master's thesis, Universität Bonn, 2001.

[10] Photonis Corporation. *XP2900 Photomultiplier Tube Data Sheet*, August 1999.

[11] U. Thoma. Physics at ELSA, Achievements and Future. *International Journal of Modern Physics A*, 20:1568–1574, 2005.

[12] H. Petry U. Lowering, B. Metsch. The light baryon spectrum in a relativistic quark model with instanton-induced quark forces. *European Physics Journal A*, 10:395–446, 2001.

[13] H. van Pee et al. Photoproduction of π^0 Mesons off Protons from the $\Delta(1232)$ Region to $E_\gamma = 3$ GeV. *European Physics Journal A*, 31:61–77, 2007.